Inorganic Chemistry

ARTICLE

pubs.acs.org/IC

Subtle Differences Between Zr and Hf in Early/Late Heterobimetallic Complexes with Cobalt

Vinay N. Setty, Wen Zhou, Bruce M. Foxman, and Christine M. Thomas*

Department of Chemistry, Brandeis University, 415 South Street, Waltham, Massachusetts 02454, United States

Supporting Information

ABSTRACT:

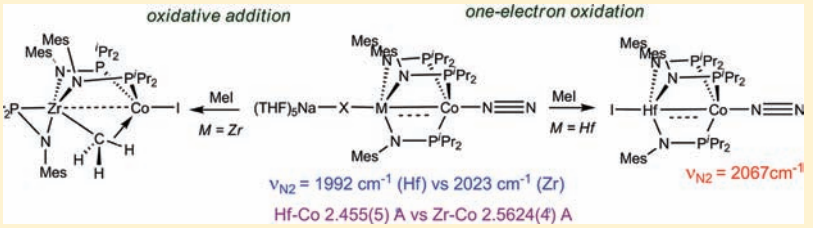

The phosphinoamide-linked Co/Hf complexes ICo(Ph_2PN^iPr)$_3$HfCl (**4**), ICo($^iPr_2PNMes$)$_3$HfCl (**5**), and ICo($^iPr_2PN^iPr$)$_3$HfCl (**6**) have been synthesized from the corresponding tris(phosphinoamide)HfCl complexes (**1**−**3**) for comparison with the recently reported tris(phosphinoamide) Co/Zr complexes. Very minor structural and electronic differences between the Zr and Hf complexes were found when the N-^{i}Pr-substituted phosphinoamide ligands [Ph_2PN^iPr]$^-$ and [$^iPr_2PN^iPr$]$^-$ were utilized. The reduction products [(THF)$_4$Na-{N_2-Co(Ph_2PN^iPr)$_3$HfCl}$_2$]Na(THF)$_6$ (**7**) and N_2-Co($^iPr_2PN^iPr$)$_3$Hf (**9**) are also remarkably similar to the corresponding Zr/Co analogues. In the case of Hf/Co and Zr/Co complexes linked by the N-Mes ligand [$^iPr_2PNMes$]$^-$ (Mes = 2,4,6-trimethylphenyl), however, more pronounced differences in structure, bonding, and reactivity are observed. While differences associated with **5** are still modest, larger variations are observed when comparing the two-electron reduction product [N_2-Co($^iPr_2PNMes$)$_3$Hf-X][Na(THF)$_5$] (**8**) with its Zr congener. In addition to structural and spectroscopic differences, vastly different reactivity is observed, with **8** undergoing one-electron oxidation to form ClHf($MesNP^iPr_2$)$_3$CoN$_2$ (**11**) in the presence of MeI, while a two-electron oxidative addition process occurs in a similar reaction with the Zr derivative. The activity of **5** toward Kumada coupling was investigated, finding significantly diminished activity in comparison to Co/Zr complexes.

INTRODUCTION

The combination of early and late transition metals in early/late heterobimetallic complexes poses a unique strategy for tuning the reactivity of transition metal complexes.[1−3] Our group and others have recently been exploring early/late heterobimetallic complexes in which the early and late transition metal are linked by phosphinoamide ligands.[4−11] It has been found that the bonds between the metals in these complexes are polar in nature, with the electron-rich late metal center donating electron density to the empty d orbital(s) on the electron-deficient early metal center.[8,9] In the case of bis(phosphinoamide)-linked Zr/Pt species, we have found that the electron-donating abilities of the ancillary ligands on Zr play a crucial role in determining the strength of the Pt→Zr interaction.[11] Nagashima and co-workers have documented a similar trend upon varying the Pt-bound ligands in similar Zr/Pt complexes.[4] We hypothesized that metal−metal interactions of this type should have a dramatic effect on the redox activity of both transition metals; indeed, we have found a ∼1 V shift to milder potentials in the reduction of the Co/Zr heterobimetallic complex ICo(Ph_2PN^iPr)$_3$ZrCl (**1**^{Zr}) as compared to its monometallic Co analogue ICo(Ph_2PNH^iPr)$_3$.[8] Moreover, we have found that upon two-electron reduction of Co/Zr heterobimetallics, complexes featuring highly polar metal−metal multiple bonds and unusual coordinatively unsaturated geometries can be isolated.[9] These reduced species are thus, highly reactive toward a variety of small molecule substrates and studies into their reactivity are ongoing.[10,12] To better understand the fundamental nature of the metal−metal interactions in early/late heterobimetallic complexes and to determine the factors that strengthen and weaken these interactions, we have begun to explore variations of both the early and late transition metal in phosphinoamide-linked heterobimetallics.

From both a steric and electronic perspective, zirconium and its heavier congener hafnium are quite similar, although hafnium complexes are often known to be less reactive than their zirconium analogues. For example, hafnium(IV) complexes have been shown, in several cases, to be more difficult to reduce than structurally similar zirconium(IV) compounds,[13−15] and in general, Hf complexes are significantly less active olefin polymerization catalysts.[16−18] However, recent literature has suggested that subtle differences between Zr and Hf may lead to substantial differences and enhanced reactivity toward C−H and N_2 activation, particularly in reduced species,

Received: March 4, 2011
Published: April 20, 2011

owing to relativistic effects promoting slightly better metal−ligand σ and π bonds in the case of Hf.[19−21] While several early/late heterobimetallic complexes featuring M→Hf interactions have been structurally characterized,[22−25] an in-depth comparative study between M/Hf and M/Zr heterobimetallic complexes has not been reported. Herein, we report the preparation of Co/Hf heterobimetallic complexes and a comparison of the metal−metal interactions in these species as compared to previously reported Co/Zr complexes.

RESULTS AND DISCUSSION

Synthesis and Characterization of Co/Hf Heterobimetallic Complexes 4−6. The tris(phosphinoamide) hafnium chloride metalloligands $(Ph_2PN^iPr)_3HfCl$ (**1**), $(^iPr_2PNMes)_3HfCl$ (**2**, Mes = 2,4,6-trimethylphenyl), and $(^iPr_2PN^iPr)_3HfCl$ (**3**) were synthesized using the same procedure as reported previously for their Zr congeners $\mathbf{1}^{Zr}$−$\mathbf{3}^{Zr}$.[6,8] The R_2PNHR' phosphinoamines were deprotonated with ^{n}BuLi, then treated with 1/3 equivalent of $HfCl_4$. Metalloligands **1**−**3** were then treated with one equivalent of CoI_2, to generate the corresponding Hf/Co heterobimetallic complexes $ICo(Ph_2PN^iPr)_3HfCl$ (**4**), $ICo(^iPr_2PNMes)_3HfCl$ (**5**), and $ICo(^iPr_2PN^iPr)_3HfCl$ (**6**), as shown in Scheme 1.[26] Similar to the Zr/Co derivatives $\mathbf{4}^{Zr}$−$\mathbf{6}^{Zr}$,[8] complexes **4**−**6** are green in color, with distinct d−d transitions in their UV−vis spectra. Single crystal X-ray diffraction data were obtained for **4**−**6**, and the resulting solid state structures are shown in Figure 1. Upon comparison of the interatomic distances and angles of **4**−**6** with the previously reported Zr/Co derivatives $\mathbf{4}^{Zr}$−$\mathbf{6}^{Zr}$, it is apparent that there are no notable differences between the structures of the ^{i}PrNHPPh$_2$ and ^{i}PrNHP^{i}Pr$_2$ complexes **4** and **6** and $\mathbf{4}^{Zr}$ and $\mathbf{6}^{Zr}$ (Table 1).[8] For example, complex **4** has a Hf−Co distance of 2.7548(5) Å, while $\mathbf{4}^{Zr}$ has a Zr−Co distance of 2.7315(5) Å, consistent with the similar covalent radii of Zr and Hf. In contrast, complex **5** has a Hf−Co distance ∼0.06 Å longer than the metal−metal distance in $\mathbf{5}^{Zr}$. Notably, the Co−Hf distances in **4**−**6** are substantially shorter than that in the lone example of a structurally characterized Co/Hf heterobimetallic complex reported to date (2.933(2) Å).[23]

Scheme 1

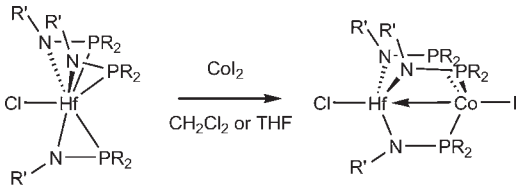

R = Ph, R' = ^{i}Pr, **1**
R = ^{i}Pr, R' = Mes, **2**
R = R' = ^{i}Pr, **3**

R = Ph, R' = ^{i}Pr, **4**
R = ^{i}Pr, R' = Mes, **5**
R = R' = ^{i}Pr, **6**

The redox behavior of Hf/Co complexes **4**−**6** was examined by cyclic voltammetry (CV) and compared with the analogous Zr/Co complexes (Figure 2, Table 1). The cyclic voltammogram of complex **4** is nearly identical to that of $\mathbf{4}^{Zr}$, characterized by a reversible two-electron reduction at −1.66 V (Figure 2). Both the Zr and Hf heterobimetallics supported by $[^iPr_2PNMes]^-$ ligands possess a reversible reduction followed by an quasi-reversible reductive process. In the case of the $[^iPr_2PN^iPr]^-$ derivatives, both the Zr and Hf complexes show two sequential irreversible reduction processes by cyclic voltammetry. Interestingly, while the reductive features of complex **5** are shifted to slightly more negative potentials than the corresponding reduction events observed for $\mathbf{5}^{Zr}$, the reductive processes in the CV of complex **6** are shifted to more positive potentials than those of $\mathbf{6}^{Zr}$. The shift of the redox events of complex **5** to more negative potentials than those of the Zr analogue is consistent with the slightly longer M−Co distance and, thus, weaker Co→Hf dative donation.

Synthesis of Dinitrogen-Bound Co/Hf Heterobimetallic Complexes 7−9 via Two-Electron Reduction. Complexes **4**−**6** were chemically reduced with excess Na/Hg amalgam to compare their reduction products with the reduced Zr/Co complexes $\mathbf{7}^{Zr}$−$\mathbf{9}^{Zr}$ (Scheme 2). Reduction of complex **4** led to a dinitrogen bound salt, $[(THF)_4Na\text{-}\{N_2\text{-}Co(Ph_2PN^iPr)_3\text{-}HfCl\}_2]Na(THF)_6$ (**7**). The solution IR of **7** revealed a $\nu(N_2)$ at 2010 cm^{-1}, ∼5 cm^{-1} lower than the $\nu(N_2)$ of the Zr analogue $\mathbf{7}^{Zr}$.[10] This slight difference in Co−N_2 backbonding is consistent with the almost negligible differences between the Zr/Co and Hf/Co complexes linked by $[Ph_2PN^iPr]^-$ ligands, as observed by M−M distance and redox potentials. The solid state structure of **7** obtained via X-ray diffraction confirms that one THF-bound Na^+ countercation associates with the lone pairs on the distal nitrogens of two symmetry-related molecules, while a second THF-bound Na^+ cation remains in an outersphere location

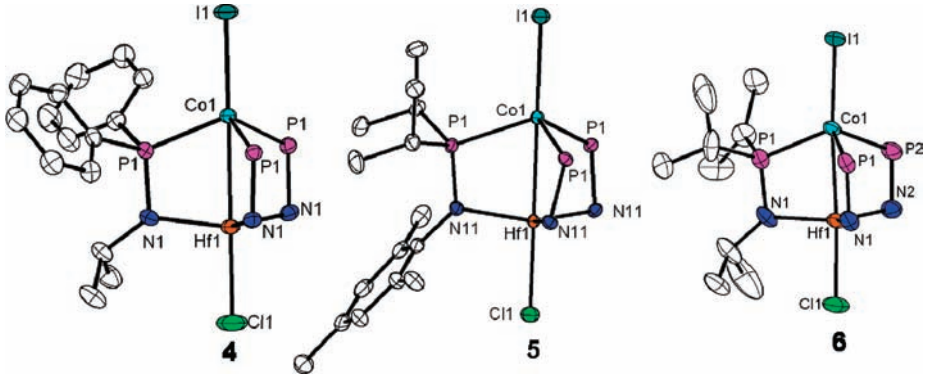

Figure 1. Displacement ellipsoid (50%) representation of **4**, **5**, and **6**. All hydrogen atoms and substituents on all but one phosphinoamide ligand have been omitted for clarity. Relevant interatomic distances (Å) and angles (deg). Complex **4**: Hf1−Co1, 2.7548(5); Hf1−N1, 2.085(2); Hf1−Cl1, 2.3512(12); Co1−P1:, 2.2886(6); Co1−I1, 2.5541(6); N1−Hf−N1, 118.57(2); P1−Co1−P1:, 107.382(19). Complex **5**: Hf1−Co1, 2.6839(5); Hf1−N11, 2.1064(15); Hf1−Cl1, 2.3972(9); Co1−P1, 2.3526(5); Co1−I1, 2.5989(5); N11−Hf1−N11, 119.155(14); P1−Co1−P1, 108.041(16). Complex **6**: Hf1−Co1, 2.6370(7); Hf1−N1, 2.090(3); Hf1−N2, 2.082(4); Hf1−Cl1, 2.427(2); Co1−P1, 2.3407(10); Co1−P2, 2.3377(16); Co1−I1, 2.5570(8); N1−Hf1−N1, 118.10(17); N1−Hf1−N2, 120.23(9); P1−Co1−P1, 106.10(5); P1−Co1−P2, 109.26(4).

dx.doi.org/10.1021/ic200445x |Inorg. Chem. 2011, 50, 4647–4655

Table 1. Comparison of Intermetallic Distances and Redox Potentials of Hf/Co Complexes 4−6 and Zr/Co Complexes 4^{Zr}−6^{Zr} and the $\nu(N_2)$ of the Reduced Derivatives 7−9 and 7^{Zr}−9^{Zr}

	M−Co distance		E (V)		$\nu(N_2)$ of reduced complex	
phosphinoamide ligand	Zr^9	Hf	Zr^8	Hf	Zr^{8-10}	Hf
$[Ph_2PN^iPr]^-$	2.7315(5) Å	2.7548(5) Å	−1.65 V[a]	−1.66 V[a]	2015 cm^{-1}[c]	2010 cm^{-1}[c]
$[^iPr_2PNMes]^-$	2.6280(5) Å	2.6839(5) Å	−1.64 V[a]	−1.69 V[a]	2023 cm^{-1}[c]	1992 cm^{-1}[c]
			−1.87 V[b]	−1.98 V[b]		
$[^iPr_2PN^iPr]^-$	2.6309(5) Å	2.6370(7) Å	−1.86 V[b]	−1.79 V[b]	2056 cm^{-1}[d]	2046 cm^{-1}[d]
			−2.07 V[b]	−1.98 V[b]		

[a] $E_{1/2}$ values are reported for these reversible redox events. [b] E^0 values are reported for these irreversible redox events. [c] Spectra were recorded in THF using a KBr solution cell. [d] Spectra were recorded in C_6H_6 using a KBr solution cell.

(Figure 3). The Hf−Co distance in **7** has contracted to 2.5470(3) Å from 2.7548(5) Å in **4**, implying a substantial increase in Hf−Co bond order upon two-electron reduction. While a solid state structure of the Zr/Co analogue 7^{Zr} could not be obtained for comparison,[10] the similarity in spectroscopic features suggests an analogous structure for the Zr and Hf derivatives.

Reduction of the $[^iPr_2PN^iPr]^-$complex **6** with excess Na/Hg also followed a similar pattern to the Zr analogue, leading to a diamagnetic N_2-bound Co/Hf species N_2-Co($^iPr_2PN^iPr)_3$Hf (**9**). While X-ray quality crystals of **9** were not obtained, the absence of resonances corresponding to bound THF in the ^{1}H NMR spectrum implies an open coordination site at Hf, directly analogous to the previously reported Zr derivative N_2-Co-($^iPr_2PN^iPr)_3$Zr (9^{Zr}).[9] In addition, combustion analysis is consistent with the proposed open coordination site formulation. In contrast to 9^{Zr}, the IR spectrum of **9** has a characteristic N_2 stretch at 2046 cm^{-1}, indicative of slightly more backbonding from Co to N_2 and, thus, a weaker Co→Hf interaction.

In contrast to the two *iso*-propylamide-substituted derivatives, substantial differences between Zr and Hf were observed upon two-electron reduction of the mesitylanilide-substituted derivative **5**. As for the Zr/Co analogue 5^{Zr},[8] reduction of **5** with excess Na/Hg in THF leads to formation of a monoanionic N_2-bound complex, [N_2-Co($^iPr_2$PNMes)$_3$Hf-X][Na(THF)$_5$] (**8**), in which the Na countercation associates closely with the Zr-bound halide (Figure 4). However, while the Zr/Co analogue 8^{Zr} undergoes rapid NaX loss to form N_2-Co($^iPr_2$PNMes)$_3$Zr-(THF) upon dissolution in benzene,[9] the Hf/Co complex **8** is insoluble in benzene and entirely inert toward a loss of NaX. Another noteworthy difference is observed by comparing the infrared N_2 stretch of **8** with 8^{Zr}: While exchange of Hf for Zr only leads to minor changes in $\nu(N_2)$ in complexes **7** and **9**, the $\nu(N_2)$ of complex **8** is ∼30 cm^{-1} lower in energy than the $\nu(N_2)$ of 8^{Zr} (1992 cm^{-1} vs 2023 cm^{-1}, Table 1). The increase in π-backbonding from Co to N_2 in **8** suggests that less Co-derived electron density is involved in π-donation to Hf. This weaker M→M interaction is also consistent with the loss in lability of the NaX moiety as Co exerts less of a *trans* influence at Hf.

Structural characterization of **8** confirmed the hypotheses derived by solution behavior. While the general formulation of **8** in the solid state is very similar to that of 8^{Zr}, there are a number of subtle but noticeable differences in interatomic distances. For example, the Co−Hf distance in **8** is elongated by ∼0.04 Å from the Co−Zr distance in 8^{Zr}. In addition, from the solid state structure of **8**, it is apparent that the dinitrogen moiety is bound more tightly to cobalt in this species than in the Zr derivative 8^{Zr}: The Co−N4 distance is

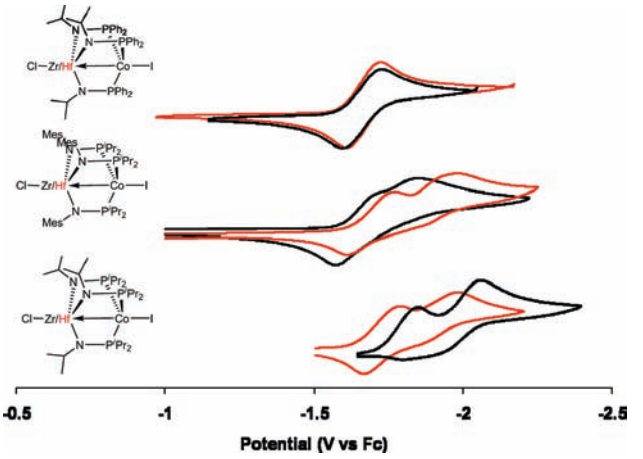

Figure 2. Cyclic voltammetry of complexes **4**−**6** and their Zr/Co analogues 4^{Zr}−6^{Zr} (4 mM analyte concentration in 0.4 M [$^nBu_4N$][PF_6] in THF, scan rate: 100 mV/s).

shorter (1.799(3) Å vs 1.8186(16) Å), and the N4−N5 distance is elongated (1.126(5) Å vs 1.120(2) Å) in **8** versus that in 8^{Zr}.[8] The structures of both **8** and 8^{Zr} contain significant disorder in the halide bound to the group IV metal. In the 8^{Zr}, the disorder was modeled accurately with occupancies of 73% I and 27% Cl, while the refined occupancies in the structure of **8** are 76% Cl and 24% I. Qualitatively, this suggests that while the NaX moiety in **8** cannot be removed irreversibly to generate a neutral N_2-Co($^iPr_2$PMesN)$_3$Hf-(THF) species, NaX dissociation must be occurring reversibly to a certain extent in solution to allow halide exchange to occur. Additional differences in structure are apparent upon inspection of the distances associated with the Hf/Zr-bound halide and the associated $Na(THF)_5^+$ cation. The Hf−Cl and Hf−I distances in **8** (2.5534(4) Å and 2.877(4) Å, respectively) are significantly shorter than the Zr−Cl and Zr−I distances in 8^{Zr} (2.690(7) Å and 2.9722(7) Å, respectively).[8] At the same time, the Na−halide distances in **8** are longer than those in 8^{Zr}, as illustrated by the Na−I distances of 3.211(4) Å and 3.2695(12) Å, respectively. These structural parameters are consistent with the greater lability of the NaX moiety in 8^{Zr} as compared to **8** and are consistent with assignment of weaker M−M bonding in the Hf derivative **8**.

Representative Reactivity of 8 as Compared to Zr Analogue 8^{Zr}. To assess the similarities and differences between the reactivity of reduced heterobimetallic complexes featuring Zr and Hf, the reactivity of the reduced Co/Hf species **8** toward oxidative addition was examined. Treatment of 8^{Zr} with MeI

dx.doi.org/10.1021/ic200445x |*Inorg. Chem.* 2011, 50, 4647–4655

Scheme 2

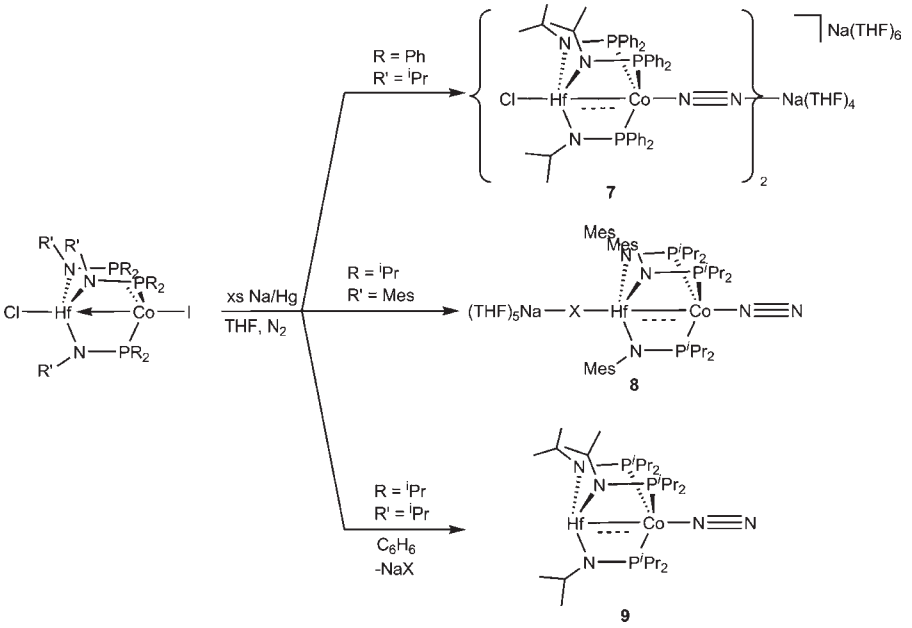

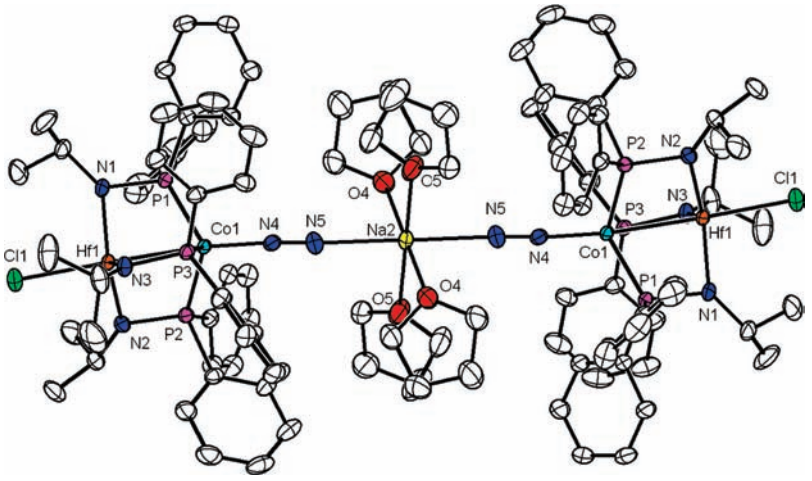

Figure 3. Displacement ellipsoid (50%) representation of **7**. All hydrogen atoms, one $Na(THF)_6$ countercation, and an outersphere THF solvent molecule have been omitted for clarity. Relevant interatomic distances (Å): Hf1−Co1, 2.5470(3); Hf1−Cl1, 2.4889(6); Hf1−N1, 2.0971(19); Hf1−N2, 2.1245(19); Hf1−N3, 2.1052(19); Co1−P1, 2.1731(6); Co1−P2, 2.1551(6); Co1−P3, 2.1639(6); Co1−N4, 1.788(2); N4−N5, 1.113(3); Na2−N5, 2.473(2).

leads to quantitative formation of the two-electron oxidized bridging methyl species $(\eta^2\text{-MesNP}^i\text{Pr}_2)\text{Zr}(\mu\text{-CH}_3)(\text{MesNP}^i\text{Pr}_2)_2\text{-CoI}$ (**10**, Scheme 3).[10] In contrast, Hf derivative **8** reacts with MeI via one-electron oxidation to yield $\text{XHf}(\text{MesNP}^i\text{Pr}_2)_3\text{CoN}_2$ (**11**). Use of labeled $^{13}CH_3I$ reveals that the byproduct of this reaction is ethane (see the Supporting Information). Complex **11** is a paramagnetic $S = 1/2$ complex, as confirmed by Evans' method ($\mu_{\text{eff}} = 2.3$ B. M.), with a characteristic $\nu(N_2)$ indicative of a weakly bound dinitrogen moiety (2067 cm^{-1}). Interestingly, the N_2 molecule is so weakly bound that it dissociates upon exposure to a vacuum, as indicated by a dramatic color change from pale orange to dark green in solution. Combustion analysis data for **11** are consistent with the absence of dinitrogen in the solid state.

X-ray crystallography confirms the structure of **11** in the solid state (Figure 5). Although complex **11** is presumed to be a 76/24 Cl/I mixture, on the basis of the disordered halide in the crystals of the starting material **8**, the solid state structure of **11** showed no sign of disorder in the halide atom bound to Hf. We attribute this to crystallization conditions, and on the basis of combustion analysis, the bulk of the sample is likely a Cl/I mixture. A comparison of the structures of the one-electron oxidized complex **11** with the fully reduced complex **8** reveals substantial differences presented in Table 2. Upon oxidation, the Hf−Co distance elongates from 2.455(5) Å to 2.5624(4) Å. The Hf−Cl distance simultaneously contracts in the absence of a strong Co→Hf interaction (2.553(4)−2.4252(8) Å). The significantly weaker bonding between Co and N_2 implied by the high frequency $\nu(N_2)$ stretch for **11** is also

dx.doi.org/10.1021/ic200445x |*Inorg. Chem.* 2011, 50, 4647–4655

Scheme 3

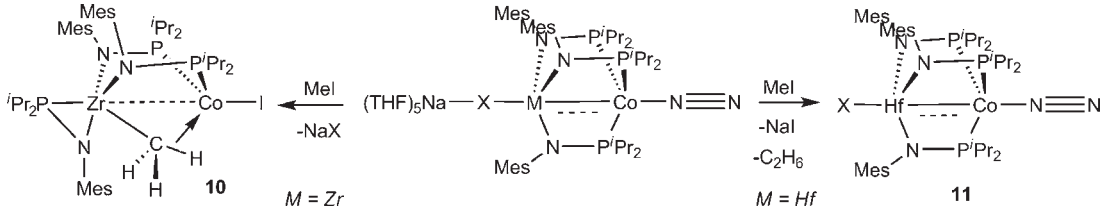

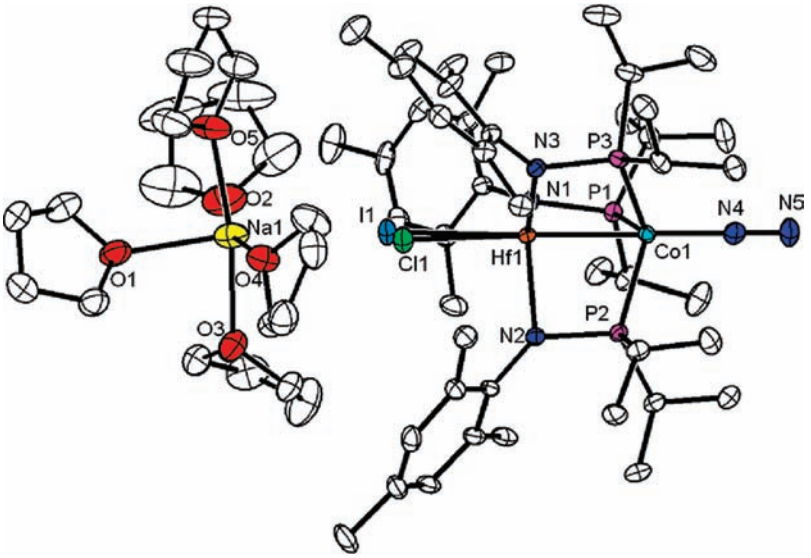

Figure 4. Displacement ellipsoid (50%) representation of **8**. All hydrogen atoms have been omitted for clarity.

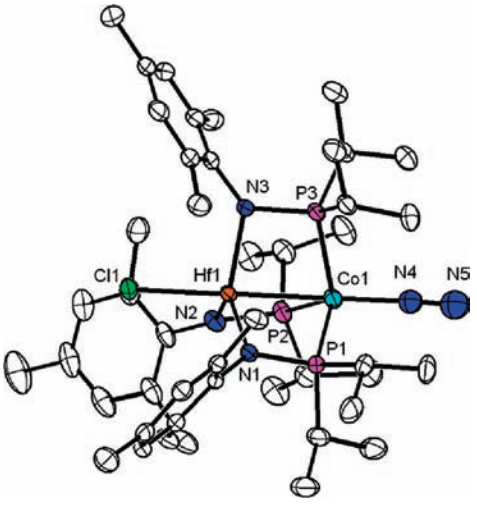

Figure 5. Displacement ellipsoid (50%) representation of **11**. All hydrogen atoms have been omitted for clarity.

evident in the solid state. The Co−N bond in **11** is ~0.05 Å longer than in **8** (1.856(4) Å vs 1.799(3) Å), while the N−N bond distance in **11** is substantially shorter than that in **8** (1.063(7) Å vs 1.126(5) Å), implying much weaker π-backbonding from Co to the N_2 π^* orbitals.

While MeI typically oxidatively adds to low valent transition metals via a two-electron process, one-electron oxidation upon the addition of alkyl halides to $[Co(CN)_5]^{3-}$ and $Cr_2(SO_4)_3$ has been well-documented.[27,28] In a more recent example, Mashima and co-workers observed the formation of $I-Pd^{I}-Mo\equiv Mo-Pd^{I}-I$ along with ethane upon the addition of excess MeI to $Pd^{0}-Mo\equiv Mo-Pd^{0}$ (where metals are connected by four 6-diphenylphosphino-2-pyridonate ligands).[29] On the basis of cyclic voltammetry data, the likely origin of the difference between the reactivity of **8** and $\mathbf{8}^{Zr}$ is a combination of the weaker Co→Hf interaction and the larger difference (0.29 V) between the two sequential reduction potentials of **8** in comparison to $\mathbf{8}^{Zr}$ (0.23 V).

We recently reported that complexes $\mathbf{4}^{Zr}-\mathbf{6}^{Zr}$ are active precatalysts for the Kumada coupling of alkyl halides with alkyl

Table 2. Comparison of Interatomic Distances in 8 and 11

	8	11
Hf−Co	2.455(5) Å	2.5624(4) Å
Hf−Cl	2.553(4) Å	2.4252(8) Å
Co−N4	1.799(3) Å	1.856(4) Å
N4−N5	1.126(5) Å	1.063(7) Å
Hf−N1	2.138(3) Å	2.108(2) Å
Hf−N2	2.128(3) Å	2.138(3) Å
Hf−N3	2.124(3) Å	2.113(2) Å
Co−P1	2.1948(11) Å	2.2786(10) Å
Co−P2	2.2010(10) Å	2.2754(9) Å
Co−P3	2.1977(11) Å	2.797(9) Å

dx.doi.org/10.1021/ic200445x |*Inorg. Chem.* 2011, 50, 4647–4655

Table 3. Comparison of Results of Kumada Coupling Reactions Using Hf/Co Complex 5 and Zr/Co Complex 5^{Zr} [12]

$$n\text{-OctMgBr} + R - X \xrightarrow[\substack{\text{TMEDA (30 mol\%)}\\ \text{THF, rt}}]{\text{cat. (5 mol \%)}} n\text{-Oct} - R$$

	yield[a]	
R−X	cat. **5**	cat. 5^{Zr}
1-bromopentane	64.2%	95.4%
2-bromobutane	10.3%	42.7%
1-chlorobutane	39.8%	45.8%
chlorocyclohexane	11.7%	55.9%

[a] Average of two values obtained via GC-MS analysis using tetradecane as an internal integration standard.

Grignard reagents and show remarkable activity toward traditionally difficult alkyl chloride substrates.[12] Notably, the monometallic analogue $ICo(Ph_2PNH^iPr)_3$ is inactive toward alkyl chlorides, implying that the early metal component plays an important role in catalysis. Given the pronounced differences in MeI oxidative addition products between Hf/Co and Zr/Co derivatives, variations in catalytic activity toward this cross-coupling reaction were also anticipated. As shown in Table , representative Hf/Co complex **5** was screened as a catalyst for the coupling of *n*-octylmagnesium bromide with both primary and secondary alkyl chloride and bromide substrates. In all cases, the yield of C−C coupled products was significantly lower when the Hf/Co complex was utilized. This difference may be attributed to either (1) the diminished M→M interaction in the Hf/Co bimetallic as compared to the Zr/Co complex or (2) a different substrate oxidative addition pathway operative in the Hf/Co case. Further studies will be needed to distinguish the role of the early metal in this catalytic process before definitive conclusions can be drawn regarding the origin of the difference in catalytic activity between Hf/Co and Zr/Co heterobimetallics.

CONCLUSIONS

In summary, in early/late heterobimetallic complexes combining group IV metals and Co (**4**−**6**, $\mathbf{4^{Zr}}$−$\mathbf{6^{Zr}}$), there are only subtle structural and electronic differences between Zr and Hf when the N-^{i}Pr-substituted phosphinoamide ligands $[Ph_2PN^iPr]^-$ and $[^iPr_2PN^iPr]^-$ are utilized. Co−M distances vary by <0.02 Å, and reduction potentials vary by <0.1 V between Co/Zr and Co/Hf complexes. The reduction products **7**/$\mathbf{7^{Zr}}$ and **9**/$\mathbf{9^{Zr}}$ are also remarkably similar. In the case of complexes linked by the N-Mes ligand $[^iPr_2PNMes]^-$, however, more pronounced differences in structure, bonding, and reactivity are observed. For example, the Co−M distance lengthens by ∼0.05 Å upon moving from Zr to Hf, and the potential difference between the first and second reduction event increases. While these differences are modest, larger differences are observed in comparing the two electron reduction products **8** and $\mathbf{8^{Zr}}$. The vastly different $\nu(N_2)$ stretches of **8** and $\mathbf{8^{Zr}}$ implicate stronger backbonding to N_2 in the Hf derivative, accompanied by a weaker Co→Hf interaction as evident in an elongated Co−Hf distance. While NaX can readily be removed from $\mathbf{8^{Zr}}$ to generate the neutral species N_2−Co(^{i}Pr$_2$PNMes)$_3$Zr(THF), the NaX unit in **8** is more tightly bound to Hf. This can be deduced by both the reluctance of NaX to dissociate and also by the shorter Hf−X contacts in the solid state structure of **8**. These differences in structure and bonding lead to vastly different reactivity, with **8** undergoing one-electron oxidation in the presence of MeI while a two-electron oxidative addition process occurs in a similar reaction with $\mathbf{8^{Zr}}$.[10] Consequently, the activity of **5** as a Kumada coupling catalyst is considerably diminished compared to that of its Co analogue.[12] While these Hf/Co complexes have not yet proven advantageous over Zr/Co complexes, their more sluggish reactivity may prove useful as a mechanistic probe in future studies.

EXPERIMENTAL SECTION

General Considerations. All syntheses reported were carried out using standard glovebox and Schlenk techniques in the absence of water and dioxygen, unless otherwise noted. Benzene, pentane, diethyl ether, tetrahydrofuran, dichloromethane, and toluene were degassed and dried by sparging with N_2 gas followed by passage through an activated alumina column using a Glass Contour Seca Solvent System. All solvents were stored over 3 Å molecular sieves. Deuterated benzene was purchased from Cambridge Isotope Laboratories, Inc., degassed via repeated freeze−pump−thaw cycles, and dried over 3 Å molecular sieves. THF-d_8 was dried over CaH_2, vacuum-transferred, and degassed via repeated freeze−pump−thaw cycles. Solvents were frequently tested using a standard solution of sodium benzophenone ketyl in tetrahydrofuran to confirm the absence of oxygen and moisture. Ph_2PNH^iPr,[30,31] $^iPr_2PNH^iPr$,[8] and $^iPr_2PNHMes$[8] were synthesized using literature procedures. All other chemicals were purchased from commercial vendors and used without further purification. NMR spectra were recorded at ambient temperature on a Varian Inova 400 MHz instrument. ^{1}H and ^{13}C NMR chemical shifts were referenced to residual solvent. ^{31}P NMR chemical shifts were referenced to 85% H_3PO_4. IR spectra were recorded on a Varian 640-IR spectrometer controlled by Resolutions Pro software. UV−vis spectra were recorded on a Cary 50 UV−vis spectrophotometer using Cary WinUV software. Elemental microanalyses were performed by Complete Analysis Laboratories, Inc., in Parsippany, New Jersey. Solution magnetic moments were measured using the Evans' method.[32,33]

Electrochemistry. Cyclic voltammetry measurements were carried out in a glovebox under a dinitrogen atmosphere in a one-compartment cell using a CH Instruments electrochemical analyzer. A glassy carbon electrode and platinum wire were used as the working and auxiliary electrodes, respectively. The reference electrode was $Ag/AgNO_3$ in THF. Solutions (THF) of electrolyte (0.40 M $[^nBu_4N][PF_6]$) and analyte (4 mM) were also prepared in the glovebox.

X-Ray Crystallography Procedures. All operations were performed on a Bruker-Nonius Kappa Apex2 diffractometer, using graphite-monochromated Mo Kα radiation. All diffractometer manipulations, including data collection, integration, scaling, and absorption corrections were carried out using the Bruker Apex2 software.[34] Preliminary cell constants were obtained from three sets of 12 frames. Structures were solved using *SIR92*[35] or SuperFlip,[36] and refinements (full-matrix-least-squares) were carried out using the Oxford University *Crystals for Windows* program.[37] All non-hydrogen atoms were refined using anisotropic displacement parameters. Experimental details are provided in Tables 4 and 5, and data collection, solution, and refinement details are supplied in the Supporting Information.

($Ph_2PN^iPr)_3HfCl$ (1). A solution of ^{i}PrNHPPh$_2$ (6.10 g, 25.0 mmol) in Et_2O (250 mL) was cooled to −78 °C. To this was added ^{n}BuLi (17.2 mL, 1.6 M in hexanes, 27.5 mmol) dropwise over 10 min. The resulting yellow/orange solution was warmed to room temperature and stirred for 2 h. The solution was then cooled again to −78 °C, and $HfCl_4$ (2.68 g, 8.30 mmol) was added portionwise as a solid. The reaction mixture was warmed to room temperature and stirred for 12 h. Volatiles were removed from the solution in vacuo, and the resulting solids were extracted with CH_2Cl_2 (20 mL) and filtered through a pad of Celite to remove LiCl.

dx.doi.org/10.1021/ic200445x |*Inorg. Chem.* 2011, 50, 4647–4655

Table 4. Crystallographic Details for Complexes 4, 5, and 6

	4	5	6
chemical formula	$C_{45}H_{51}ClCoHfIN_3P_3$	$C_{45}H_{75}ClCoHfIN_3P_3$	$C_{27}H_{63}ClCoHfIN_3P_3$
fw	1126.62	1150.81	922.52
T (K)	120	120	120
λ (Å)	0.71073	0.71073	0.71073
a (Å)	20.8180(3)	12.0541(3)	15.1818(4)
b (Å)	20.8180(3)	12.0541(3)	18.1649(5)
c (Å)	20.8180(3)	19.7252(7)	13.5297(4)
α (deg)	90	90	90
β (deg)	90	90	90
γ (deg)	90	120	90
V (Å^3)	9022.3(2)	2482.11(12	3731.17.(18)
space group	$Pa\bar{3}$	P-3	$Pnma$
Z	8	2	4
D_{calcd} (g/cm^3)	1.659	1.540	1.642
μ (mm^{-1})	3.552	3.229	4.273
R1, wR2[a] ($I > 2\sigma(I)$)	0.0232, 0.0534	0.0200, 0.0431	0.0321, 0.0624

[a] $R1 = \Sigma||F_o| - |F_c||/\Sigma|F_o|$, $wR2 = \{\Sigma[w(F_o^2 - F_c^2)_2]/\Sigma[w(F_o^2)^2]\}^{1/2}$.

Table 5. Crystallographic Details for Complexes 7, 8, and 11

	7·THF	8	11·1.5Et$_2$O
chemical formula	$C_{69}H_{99}ClCoHfN_5NaO_6P_3$	$C_{65}H_{115}Cl_{0.76}CoHfI_{0.24}N_5NaO_5P_3$	$C_{51}H_{90}ClCoHfI_{0.02}N_{4.97}O_{1.5}P_3$
fw	1483.36	1457.79	1164.62
T (K)	120	120	120
λ (Å)	0.71073	0.71073	0.71073
a (Å)	12.7902(8)	14.6354(4)	27.9112(11)
b (Å)	13.8837(8)	24.6754(7)	15.4306(6)
c (Å)	22.7745(14)	19.2156(6)	26.3171(10)
α (deg)	99.384(3)	90	90
β (deg)	102.512(3)	90.2243(16	90
γ (deg)	100.827(3)	90	90
V (Å^3)	3789.3(4)	6939.4(3)	11334.4(8)
space group	P-1	$P121/n1$	$Pbcn$
Z	2	4	8
D_{calcd} (g/cm^3)	1.300	1.395	1.365
μ (mm^{-1})	1.741	1.997	2.303
R1, wR2[a] ($I > 2\sigma(I)$)	0.0287, 0.0724	0.0398, 0.0645	0.0318, 0.0611

[a] $R1 = \Sigma||F_o| - |F_c||/\Sigma|F_o|$, $wR2 = \{\Sigma[w(F_o^2 - F_c^2)_2]/\Sigma[w(F_o^2)^2]\}^{1/2}$.

The volatiles were removed from the resulting filtrate in vacuo, and the resulting solids were washed with pentane (3 × 50 mL) to yield analytically pure **1** as a white solid (5.437 g, 69.6%). ^{1}H NMR (400 MHz, C_6D_6): δ 7.46 (m, 12H, *o*-Ph), 6.96 (m, 12H, *m*-Ph), 6.94 (m, 6H, *p*-Ph), 4.22 (m, 3H, C*H*(CH$_3$)$_2$), 1.52 (d, J = 6 Hz, 18H, CH(C*H*$_3$)$_2$). ^{31}P{^{1}H} NMR (161.8 MHz, C_6D_6): δ −4.2 (s). ^{13}C NMR (100.5 MHz, C_6D_6): δ 137.4 (d, $^1J_{P-C}$ = 11.5 Hz, *ipso*-Ph), 134.0 (d, m, *o*-Ph), 129.6 (s, *p*-Ph), 128.3 (s, *m*-Ph), 53.7 (s, NCH(CH$_3$)$_2$), 27.6 (s, NCH(CH$_3$)$_2$).

(^{i}Pr$_2$PNMes)$_3$HfCl (2). A solution of MesNHP^{i}Pr$_2$ (12.198 g, 48.5 mmol) in Et$_2$O (200 mL) was cooled to −78 °C. To this was added ^{n}BuLi (33.3 mL, 1.6 M in hexanes, 53.3 mmol) dropwise over 10 min. The resulting yellow/orange solution was warmed to room temperature and stirred for 2 h. The solution was then cooled again to −78 °C, and HfCl$_4$ (5.158 g, 16.0 mmol) was added portionwise as a solid. The reaction mixture was warmed to room temperature and stirred for 12 h. Volatiles were removed from the solution in vacuo, and the resulting solids were extracted with CH$_2$Cl$_2$ (20 mL) and filtered through a pad of Celite to remove LiCl. The volatiles were removed from the resulting filtrate in vacuo, and the resulting solids were washed with pentane (3 × 50 mL) to yield analytically pure **2** as a white solid (8.276 g, 53.6%). ^{1}H NMR (400 MHz, C_6D_6): δ 6.87 (s, 6H, Mes), 2.55 (s, 18H, Mes-Me), 2.41 (m, 6H, PC*H*(CH$_3$)$_2$), 2.22 (s, 9H, Mes-Me), 1.30 (m, 18H, PCH(C*H*$_3$)$_2$), 1.17 (m, 18H, PCH(C*H*$_3$)$_2$). ^{31}P{^{1}H} NMR (161.8 MHz, C_6D_6): δ 16.6 (s). ^{13}C NMR (100.5 MHz, C_6D_6): δ 148.7 (*ipso*-Mes), 134.2 (*o*-Mes), 132.3 (*p*-Mes), 129.6 (*m*-Mes), 38.8 (PCH(CH$_3$)$_2$), 22.1 (PCH(CH$_3$)$_2$ + MesMe overlapping), 21.3 (PCH(CH$_3$)$_2$ + MesMe overlapping). Anal. Calcd for $C_{45}H_{75}ClHfN_3P_3$: C, 56.01; H, 7.83; N, 4.35. Found: C, 56.06; H, 7.96; N, 4.51.

(^{i}Pr$_2$PN^{i}Pr)$_3$HfCl (3). A solution of ^{i}PrNHP^{i}Pr$_2$ (4.496 g, 25.7 mmol) in Et$_2$O (150 mL) was cooled to −78 °C. To this was added ^{n}BuLi (14.8 mL, 1.6 M in hexanes, 26.9 mmol) dropwise over 10 min. The resulting yellow/orange solution was warmed to room temperature

dx.doi.org/10.1021/ic200445x |*Inorg. Chem.* 2011, 50, 4647–4655

and stirred for 2 h. The solution was then cooled again to −78 °C, and $HfCl_4$ (2.739 g, 8.55 mmol) was added portionwise as a solid. The reaction mixture was warmed to room temperature and stirred for 12 h. Volatiles were removed from the solution in vacuo, and the resulting solids were extracted with CH_2Cl_2 (20 mL) and filtered through a pad of Celite to remove LiCl. The volume of the filtrate was reduced to 5 mL in vacuo. The resulting supersaturated solution was layered with pentane and cooled to −35 °C to yield analytically pure colorless crystals of **3** (3.126 g, 49.6%). ^{1}H NMR (400 MHz, C_6D_6): δ 4.09 (m, 3H, NC*H*-$(CH_3)_2$), 2.16 (m, 6H, PC*H*$(CH_3)_2$), 1.59 (d, J = 6.4 Hz, 18H, NCH$(CH_3)_2$), 1.11−1.25 (m, 36H, PCH$(CH_3)_2$). ^{31}P{^{1}H} NMR (161.8 MHz, C_6D_6): δ 7.5 (s). ^{13}C NMR (100.5 MHz, C_6D_6): δ 53.1 (NCH$(CH_3)_2$), 29.1 (NCH$(IH_3)_2$), 27.5 (PCH$(CH_3)_2$), 22.2 (PCH$(CH_3)_2$, $^1J_{PC}$ = 11 Hz), 19.7 (PCH$(CH_3)_2$). Anal. Calcd for $C_{27}H_{63}ClHfN_3P_3$: C, 44.02; H, 8.62; N, 5.70. Found: C, 43.95; H, 8.58; N, 5.44.

ICo(Ph$_2$PN^{i}Pr)$_3$HfCl (4). Solid **1** (5.437 g, 5.78 mmol) and solid CoI_2 (1.82 g, 5.78 mmol) were combined in THF (200 mL) and stirred for 12 h at room temperature. The resulting dark green reaction solution was filtered through Celite, and solvent was removed from the volatiles in vacuo. The remaining green solids were extracted with toluene (10 mL) and filtered through Celite. The filtrate was cooled to −35 °C overnight to yield **4** as dark green crystalline solids (5.771 g, 88.7%). Crystals for X-ray diffraction were grown by cooling a toluene/pentane solution to −35 °C. ^{1}H NMR (400 MHz, C_6D_6): δ 14.5 (br s, Ph), 5.1 (br, (C*H*$(CH_3)_2$), 1.2 (br s, (CH$(CH_3)_2$), −5.5 (br, Ph), −7.3 (br s, Ph). UV−vis (λ, nm (ε, cm^{-1} M^{-1})): 578 (120), 690 (180), 708 (170), 735 (190), 750 (220), 776 (300), 867 (350). Evans' method (C_6D_6): 3.0 μ_B. Anal. Calcd for $C_{45}H_{51}ClCoHfIN_3P_3$: C, 47.97; H 4.56, N, 3.74. Found: C, 47.94; H 4.67, N, 3.71.

ICo(^{i}Pr$_2$PNMes)$_3$HfCl (5). Solid **2** (0.0846 g, 0.0877 mmol) and solid CoI_2 (0.0274 g, 0.0877 mmol) were combined in CH_2Cl_2 (4 mL) and stirred for 48 h at room temperature. The resulting dark green reaction solution was filtered through Celite and solvent was removed from the volatiles in vacuo. The remaining green solids were washed with copious pentane and dried in vacuo to yield analytically pure **5** as a green powder (0.0864 g, 85.7%). Cyrstals suitable for X-ray diffraction were grown from CH_2Cl_2 and Et_2O at room temperature. ^{1}H NMR (400 MHz, C_6D_6): δ 13.6 (br s, PCH(C*H*$_3)_2$), 7.0 (Mes-Me), 2.8 (br s, PCH(C*H*$_3)_2$), 2.1 (Mes-Me), −2.0 (br, Mes-Ar) . UV−vis (λ, nm (ε, cm^{-1} M^{-1})): 342 (6900), 382 (4800), 648 (150), 783 (140), 802 (150), 890 (320). Evans' method (C_6D_6): 3.3 μ_B. Anal. Calcd for $C_{45}H_{75}ClCoHfIN_3P_3$: C, 46.97; H, 6.57; N, 3.65. Found: C, 46.87; H, 6.73; N, 3.59

ICo(^{i}Pr$_2$PN^{i}Pr)$_3$HfCl (6). Solid **3** (1.1373 g, 1.544 mmol) and solid CoI_2 (0.483 g, 1.544 mmol) were combined in CH_2Cl_2 (20 mL) and stirred for 48 h at room temperature. The resulting dark green reaction solution was filtered through Celite, and solvent was removed from the volatiles in vacuo. The remaining green solids were extracted with toluene (10 mL) and filtered through Celite. The filtrate was cooled to −35 °C overnight to yield **6** as dark green crystalline solids (0.427 g, 30.0%). Crystals suitable for X-ray diffraction were grown from toluene/pentane at −35 °C. ^{1}H NMR (400 MHz, C_6D_6): δ 72 (br s, PC*H*-$(CH_3)_2$), 8.6 (br s, PCH(C*H*$_3)_2$), 5.1 (br s, NC*H*$(CH_3)_2$), 1.7 (br s, NCH(C*H*$_3)_2$), −2.2 (br s, PCH(C*H*$_3)_2$) . UV−vis (λ, nm (ε, cm^{-1} M^{-1})): 337 (3100), 439 (670), 691 (210), 728 (250), 743 (280), 769 (350), 887 (170). Evans' method (C_6D_6): 3.0 μ_B. Anal. Calcd for $C_{27}H_{63}ClCoHfIN_3P_3$: C, 35.15; H, 6.88; N, 4.55. Found: C, 35.43; H, 7.01; N, 4.70.

[(THF)$_4$Na{N$_2$Co(Ph$_2$PN^{i}Pr)$_3$HfCl}$_2$]Na(THF)$_6$] (7). A 0.5% Na/Hg amalgam was prepared from 32 mg of Na (1.4 mmol) and 6.5 g of Hg. To this vigorously stirred amalgam in 5 mL of THF was added a solution of **4** (0.635 g, 0.564 mmol) in THF (2 mL). The solution immediately began to change color from green to red. After 2 h, the resulting red solution was filtered away from the amalgam, and the solvent was removed from the filtrate in vacuo. Solids were extracted back into THF and filtered through Celite. Layering the resulting concentrated red solution with pentane and cooling to −35 °C resulted in red crystals of **7** (0.480 g, 60.4%). ^{1}H NMR (400 MHz, THF-d_8): δ 7.42 (m, 24H, *o*-Ph), 6.84 (m, 12H, *p*-Ph), 6.72 (m, 24H, *m*-Ph), *p*-Ph), 4.22 (m, 6H, C*H*$(CH_3)_2$), 3.54 (m, 8H, THF), 1.68 (m, 8H, THF), 1.78 (d, J = 6.4 Hz, 36H, CH(C*H*$_3)_2$). ^{31}P{^{1}H} NMR (162 MHz, C_6D_6): δ 44 ppm (br s). ^{13}C NMR (100.5 MHz, THF): δ 143.6 (m, *ipso*-Ph), 133.0 (s, *o*-Ph), 126.3 (s, *m*-Ph), 125.8 (s, *m*-Ph), 49.8 (s, NCH$(CH_3)_2$), 27.0 (s, NCH(C*H*$_3)_2$. IR (KBr solution cell, THF): 2010 cm^{-1}. UV−vis (λ, nm (ε, cm^{-1} M^{-1})): 445 (14 600), 672 (190). Satisfactory combustion analysis data could not be obtained on repeated attempts. This is likely a result of the extreme sensitivity of this complex to air and moisture and the lability of the bound N_2 unit.

N$_2$Co(^{i}Pr$_2$PNMes)$_3$HfX-Na(THF)$_5$ (8). A 0.5% Na/Hg amalgam was prepared from 26 mg of Na (1.1 mmol) and 5.1 g of Hg. To this vigorously stirred amalgam in 5 mL of THF was added a solution of **5** (0.511 g, 0.444 mmol) in THF (2 mL). The solution immediately began to change color from green to red/orange. After 2 h, the resulting red/orange solution was filtered away from the amalgam, and the solvent was removed from the filtrate in vacuo. Solids were extracted back into THF and filtered through Celite. Layering the resulting concentrated red solution with pentane and cooling to −35 °C resulted in orange crystals of **8** (0.487 g, 74.5%). Crystals suitable for X-ray diffraction were grown by vapor diffusion of pentane into a concentrated THF solution of N$_2$Co(^{i}Pr$_2$PNMes)$_3$HfX-Na(THF)$_5$ at −35 °C. ^{1}H NMR (400 MHz, THF-d_8): δ 6.55 (s, 6H, Mes), 3.61 (Na-THF), 2.76 (m, 6H, PC*H*-$(CH_3)_2$), 2.38 (s, 18H, Mes-Me), 2.10 (s, 9H, Mes-Me), 1.50 (m, 18H, PCH(C*H*$_3)_2$), 1.37 (m, 18H, PCH(C*H*$_3)_2$). ^{31}P{^{1}H} NMR (162 MHz, C_6D_6): δ 50.1 (br s). ^{13}C NMR (100.5 MHz, THF): δ 135.0 (s, *o*-Mes), 134.9 (s, *ipso*-Mes), 128.7 (s, *p*-Mes), 127.8 (s, *m*-Mes), 44.5 (m, PCH$(CH_3)_2$), 25.0 (PCH$(CH_3)_2$ overlapping with THF peak), 23.8 (s, MesMe) 22.8 (s, PCH(C*H*$_3)_2$), 20.1 (s, MesMe). IR (KBr solution cell, THF): 1992 cm^{-1}. UV−vis (λ, nm (ε, cm^{-1} M^{-1})): 441 (1312). Satisfactory combustion analysis data could not be obtained on repeated attempts. This is likely a result of the extreme sensitivity of this complex to air and moisture and the lability of the bound N_2 unit.

N$_2$Co(^{i}Pr$_2$PN^{i}Pr)$_3$Hf (9). A 0.5% Na/Hg amalgam was prepared from 10 mg of Na (0.45 mmol) and 2.0 g of Hg. To this vigorously stirred amalgam in 5 mL of THF was added a solution of **6** (0.149 g, 0.179 mmol) in THF (2 mL). The solution immediately began to change color from green to red. After 2 h, the resulting red solution was filtered away from the amalgam, and the solvent was removed from the filtrate in vacuo. Solvent was extracted into C_6H_6 and filtered through Celite. Solvent was removed in vacuo to yield analytically pure product as a red powder (0.0805 g, 58.3%). Crystals suitable for X-ray diffraction were grown via vapor diffusion of pentane into a concentrated solution of **9** in THF at −35 °C. ^{1}H NMR (400 MHz, C_6D_6): δ 3.67 (m, 3H, NC*H*$(CH_3)_2$), 2.76 (m, 6H, PC*H*$(CH_3)_2$), 1.42 (m, 36H, PCH-$(CH_3)_2$), 1.11 (d, J = 4 Hz, 18H, NCH(C*H*$_3)_2$), 1.11−1.25 (m, 36H, PCH(C*H*$_3)_2$). ^{31}P{^{1}H} NMR (162 MHz, C_6D_6): δ 38.7 ppm (br s). ^{13}C NMR (100.5 MHz, C_6D_6): δ 48.4 (NCH$(CH_3)_2$), 32.0 (PCH$(CH_3)_2$), 31.1 (PCH(C*H*$_3)_2$), 21.4 (NCH(C*H*$_3)_2$), 20.0 (PCH(C*H*$_3)_2$). IR (KBr solution cell, C_6H_6): 2046 cm^{-1}. UV−vis (λ, nm (ε, cm^{-1} M^{-1})): 296 (10000), 336 (6000), 442 (1000), 520 (650), 755 (80). Anal. Calcd for $C_{27}H_{63}CoHfN_5P_3$: C, 41.14; H, 8.06; N, 8.89. Found: C, 41.25; H, 8.19; N, 8.83.

N$_2$Co(^{i}Pr$_2$NMes)$_3$HfX (11). Complex **8** (0.1309 g, 0.0913 mmol) was dissolved in THF (5 mL). To this was added dropwise a dilute THF solution of MeI (4.5 μL, 0.073 mmol) in 2 mL of THF. A substoichiometric amount of MeI resulted in the most satisfactory yields owing to the difficulty in determining the exact MW of samples of **8** due to the mixture of Cl^-/I^-. After 30 min of stirring at room temperature,

volatiles were removed from the mixture in vacuo. The remaining orange solids were extracted with benzene (3 mL) and filtered through Celite to remove NaX salts. Volatiles were removed in vacuo to yield spectroscopically pure product as a green/brown powder (0.0587 g, 70.3% based on MeI). Note: In solution, N_2 is bound, leading to an orange product. Upon exposure to a vacuum, a color change to green was observed, suggesting dissociation of N_2 (consistent with elemental analysis results). Crystals suitable for X-ray diffraction were grown via slow evaporation of a concentrated Et_2O solution at −35 °C. ^{1}H NMR (400 MHz, C_6D_6): δ 7.75 (s, *m*-Mes), 5.82 (s, ^{i}Pr-Me), 5.14 (br s, ^{i}Pr-CH), 2.92 (s, ^{i}Pr-Me), 2.24 (s, *p*-Mes), −1.70 (s, *o*-Mes). IR (KBr solution cell, C_6H_6): 2067 cm^{-1}. Evans' method (C_6D_6): 2.3 μ_B. Anal. Calcd for $C_{45}H_{75}CoHfI_{0.24}Cl_{0.76}N_3P_3$: C, 50.22; H, 6.98; N, 3.91. Found: C, 48.79; H, 6.88; N, 3.61. Note: Repeated combustion analysis showed evidence for a loss of dinitrogen prior to analysis. Satisfactory analysis was obtained if a 76:24 Cl/I mixture (resulting from composition of the I/Cl mixtures in the starting material, **8**) is considered.

Typical Procedure for Kumada Coupling Reactions. In a nitrogen-filled glovebox, alkyl halide (0.47 mmol) and TMEDA (16.5 mg, 0.14 mmol, 30 mol %) were weighed into a 20 mL vial. Dry THF (7 mL) and complex **5** (0.024 mmol, 5 mol %) were added, and the mixture was stirred for 10 min. To this mixture, *n*-OctMgBr (2 M in Et_2O, 0.28 mL, 0.56 mmol) was added by syringe pump at a rate of 2 mL per hour. Upon completion of this addition, the reaction was removed from the glovebox, and saturated aqueous NH_4Cl was added to quench the reaction. The organic layer was passed through a silica plug, and the resulting mixture was analyzed using GC-MS. Yields were determined via comparison to an internal standard (tetradecane).

■ ASSOCIATED CONTENT

Supporting Information. CIF files and additional crystallographic details for complexes **4**−**8** and **11**. This material is available free of charge via the Internet at http://pubs.acs.org.

■ AUTHOR INFORMATION

Corresponding Author
*E-mail: thomasc@brandeis.edu.

■ ACKNOWLEDGMENT

This material is based upon work supported by the Department of Energy under Award No. DE-SC0004019. We also thank Brandeis University for funding this work.

■ REFERENCES

(1) Stephan, D. W. *Coord. Chem. Rev.* **1989**, *95*, 41–107.
(2) Wheatley, N.; Kalck, P. *Chem. Rev.* **1999**, *99*, 3379–3420.
(3) Gade, L. H. *Angew. Chem., Int. Ed.* **2000**, *39*, 2658–2678.
(4) Nagashima, H.; Sue, T.; Oda, T.; Kanemitsu, A.; Matsumoto, T.; Motoyama, Y.; Sunada, Y. *Organometallics* **2006**, *25*, 1987–1994.
(5) Sunada, Y.; Sue, T.; Matsumoto, T.; Nagashima, H. *J. Organomet. Chem.* **2006**, *691*, 3176–3182.
(6) Sue, T.; Sunada, Y.; Nagashima, H. *Eur. J. Inorg. Chem.* **2007**, *2007*, 2897–2908.
(7) Tsutsumi, H.; Sunada, Y.; Shiota, Y.; Yoshizawa, K.; Nagashima, H. *Organometallics* **2009**, *28*, 1988–1991.
(8) Greenwood, B. P.; Forman, S. I.; Rowe, G. T.; Chen, C.-H.; Foxman, B. M.; Thomas, C. M. *Inorg. Chem.* **2009**, *48*, 6251–6260.
(9) Greenwood, B. P.; Rowe, G. T.; Chen, C.-H.; Foxman, B. M.; Thomas, C. M. *J. Am. Chem. Soc.* **2010**, *132*, 44–45.
(10) Thomas, C. M.; Napoline, J. W.; Rowe, G. T.; Foxman, B. M. *Chem. Commun.* **2010**, *46*, 5790–5792.
(11) Cooper, B. G.; Fafard, C. M.; Foxman, B. M.; Thomas, C. M. *Organometallics* **2010**, *29*, 5179–5186.
(12) Zhou, W.; Napoline, J. W.; Thomas, C. M. *Eur. J. Inorg. Chem.* **2011**, DOI: 10.1002.ejic.201100109.
(13) Lappert, M. F.; Raston, C. L. *J. Chem. Soc., Chem. Commun.* **1980**, 1284–1285.
(14) Silveira, F.; Simplício, L. M. T.; Rocha, Z. N. d.; Santos, J. H. Z. d. *Appl. Catal., A* **2008**, *344*, 98–106.
(15) Lappert, M. F.; Raston, C. L.; Skelton, B. W.; White, A. H. *J. Chem. Soc., Dalton Trans.* **1984**, 893–902.
(16) Weiss, K.; Neugebauer, U.; Blau, S.; Lang, H. *J. Organomet. Chem.* **1996**, *520*, 171–179.
(17) Jany, G.; Gustafsson, M.; Repo, T.; Aitola, E.; Dobado, J. A.; Klinga, M.; Leskelä, M. *J. Organomet. Chem.* **1998**, *553*, 173–178.
(18) Ransom, P.; Ashley, A. E.; Brown, N. D.; Thompson, A. L.; O'Hare, D. *Organometallics* **2011**, *30*, 800−814.
(19) Marschner, C. *Angew. Chem., Int. Ed.* **2007**, *46*, 6770–6771.
(20) Krueger, C.; Mueller, G.; Erker, G.; Dorf, U.; Engel, K. *Organometallics* **1985**, *4*, 215–223.
(21) Jacobsen, H.; Berke, H.; Brackemeyer, T.; Eisenblätter, T.; Erker, G.; Fröhlich, R.; Meyer, O.; Bergander, K. *Helv. Chim. Acta* **1998**, *81*, 1692–1709.
(22) Oishi, M.; Kato, T.; Nakagawa, M.; Suzuki, H. *Organometallics* **2008**, *27*, 6046–6049.
(23) Lang, H.; Herres, M.; Imhof, W. *J. Organomet. Chem.* **1994**, *465*, 283–287.
(24) Gelmini, L.; Stephan, D. W. *Organometallics* **1988**, *7*, 849–855.
(25) Baker, R. T.; Fultz, W. C.; Marder, T. B.; Williams, I. D. *Organometallics* **1990**, *9*, 2357–2367.
(26) Much like the reactions to form $\mathbf{4}^{Zr}$−$\mathbf{6}^{Zr}$, the fate of the second I^- ion and the origin of the reduction from Co^{II} to Co^{I} has not been unambiguously determined. However, since similar products are not formed from $CoCl_2$, we suggest that the $2I^- \rightarrow I_2$ redox couple plays a role in the reduction of Co^{I}. The formation of I_2 could not be monitored, however, since I_2 reacts readily with the tris(phosphinoamide)MCl starting materials.
(27) Halpern, J. *Acc. Chem. Res.* **1970**, *3*, 386–392.
(28) Castro, C. E.; Kray, W. C. *J. Am. Chem. Soc.* **1963**, *85*, 2768–2773.
(29) Mashima, K.; Shima, A.; Nakao, K.; Fukumoto, A.; Kaneda, Y.; Kusumi, Y. *Inorg. Chem.* **2009**, *48*, 1879–1886.
(30) Sisler, H.; Smith, N. *J. Org. Chem.* **1961**, *26*, 611–613.
(31) Poetschke, N.; Nieger, M.; Khan, M. A.; Niecke, E.; Ashby, M. T. *Inorg. Chem.* **1997**, *36*, 4087–4093.
(32) Sur, S. K. *J. Magn. Reson.* **1989**, *82*, 169–173.
(33) Evans, D. F. *J. Chem. Soc.* **1959**, 2003–2005.
(34) *Apex 2, Version 2 User Manual, M86-E01078*; Bruker Analytical X-ray Systems: Madison, WI, 2006.
(35) Altomare, A.; Cascarano, G.; Giacovazzo, G.; Guagliardi, A.; Burla, M. C.; Polidori, G.; Camalli, M. *J. Appl. Crystallogr.* **1994**, *27*, 435–436.
(36) Palatinus, L.; Chapuis, G. *J. Appl. Crystallogr.* **2007**, *40*, 786–790.
(37) Betteridge, P. W.; Carruthers, J. R.; Cooper, R. I.; Prout, K.; Watkin, D. J. *J. Appl. Crystallogr.* **2003**, *36*, 1487.